EurJIC
European Journal of Inorganic Chemistry

Research Article
doi.org/10.1002/ejic.202500212

Chemistry Europe
European Chemical Societies Publishing

www.eurjic.org

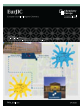

Unveiling Solvent-Dependent Divergent Hydrogen Production Pathways during the Dehydrogenation of Formic Acid Using N,N′-Iminopyridine Ruthenium(II) Complexes

Thabiso Mphuti, Rotondwa Mphephu, Moegamat Joseph, and Andrew J. Swarts*

The preparation of a panel of cationic, half-sandwich iminopyridine ruthenium(II) complexes of the type [(**L1**)RuCl(*p*-cymene)]Cl (**C1**–**C11**) is reported, where L = substituted *N*-phenyl-1-(2-pyridinyl)methanimine ligand derivates (**L1**–**L9**) and their efficiency in the catalytic dehydrogenation of formic acid (FA). The activity could be correlated with the nature of the substituent on the imine nitrogen and the solubility of the complexes in water, with **C1** exhibiting the highest initial turnover frequency (TOF) of 281 hr^{-1} at 90 °C. Kinetic and mechanistic investigations are undertaken in dimethyl sulfoxide (DMSO) and H_2O, revealing that the proton source in the hydrogen production step is solvent-dependent. FA is found to be responsible for H_2 formation in DMSO, and H_3O^+ ions are involved in generating H_2 in water. Complex **C1** is more stable in water, as it maintains efficient gas evolution for 16 cycles without any deactivation, reaching a turnover number (TON) of 13 791. Furthermore, **C1** is active, although with reduced activity (TOF = 43 hr^{-1}), for over 34 h when operated under continuous FA addition conditions.

1. Introduction

Efforts to implement a "hydrogen economy" have often been impeded by a lack of suitable storage systems for hydrogen gas. Its low volumetric density (0.08988 g L^{-1} at 1 atm) makes it difficult to store and transport using existing infrastructure for fuels.[1] An alternative approach to attain this objective is the introduction of liquid organic hydrogen carriers (LOHCs) as potential H_2 energy vectors. LOHCs such as formic acid (FA, HCOOH) can undergo reversible hydrogenation and dehydrogenation cycles, which enable hydrogen storage and release.[2] FA is a liquid under ambient conditions, enabling easy storage, handling, and transportation. It has a moderately high hydrogen content (4.4 wt%) and a high energy density (1.77 kWh L^{-1}).[3] The dehydrogenation of FA to generate H_2 gas and carbon dioxide using a homogeneous complex was first described by Coffey more than half a century ago.[4] The use of heterogeneous[5,6] and homogeneous catalyst systems[7,8] toward FA dehydrogenation (FADH) is well documented in the literature. Although heterogeneous catalysts offer excellent recovery, they do not provide the superior catalytic activity achieved by homogeneous catalysts. Since the initial seminal reports,[9,10] several state-of-the-art complexes based on iron (**I**), iridium (**II**, **III**), and ruthenium (Ru, **IV**) have been reported for the catalytic dehydrogenation of FA. Hazari and Schneider reported an iron complex, **I**, based on an earth-abundant metal, generating turnover number (TON) and turnover frequency (TOF) of 980 000 and 200 000, respectively.[11] Precious metal-containing **II**, **III**, and **IV** could generate TONs of up to 3 000 000, allowing access to industrially competitive FADH catalysts (**Figure 1**).[7,12,13] These exceptional catalyst systems have led to a surge in the number of investigations seeking to access high-performance FADH catalysts (Figure 1). However, most of them require the inclusion of organic solvents and sophisticated ligand scaffolds for efficient gas evolution, while exhibiting poor solubility and activity toward FA dehydrogenation in water as a solvent.[14–16] To date, only a few ruthenium-based complexes that can function in water have been reported (Figure 1).[17–19] Huang and co-workers reported the dehydrogenation of FA in water using a Ru complex, **V**, bearing an N,N′-diimidazole ligand in the absence of organic additives.[17] A TOF of 12 000 hr^{-1} and a TON of 350 000 at 90 °C were obtained from an aqueous solution of FA and sodium formate (HCOONa). In addition, they demonstrated the production of high-pressure H_2 and CO_2 up to 24.0 MPa (3480 psi). Singh and coworkers reported H_2 production from the dehydrogenation of FA over pyridinemethanol-based Ru complexes, **VI**, in water.[18] The complexes exhibited high stability in water and could be recycled up to seven times with a total TON of 6050. He and coworkers reported the dehydrogenation of aqueous FA by a

T. Mphuti, R. Mphephu, M. Joseph, A. J. Swarts
Molecular Sciences Institute
School of Chemistry
University of the Witwatersrand
PO Wits
2050 Johannesburg, South Africa
E-mail: andrew.swarts@wits.ac.za

M. Joseph
Department of Chemistry and Polymer Science
Stellenbosch University
Private Bag 1, Matieland, 7601 Stellenbosch, South Africa

Supporting information for this article is available on the WWW under https://doi.org/10.1002/ejic.202500212

Research Article
doi.org/10.1002/ejic.202500212

Chemistry Europe
European Chemical Societies Publishing

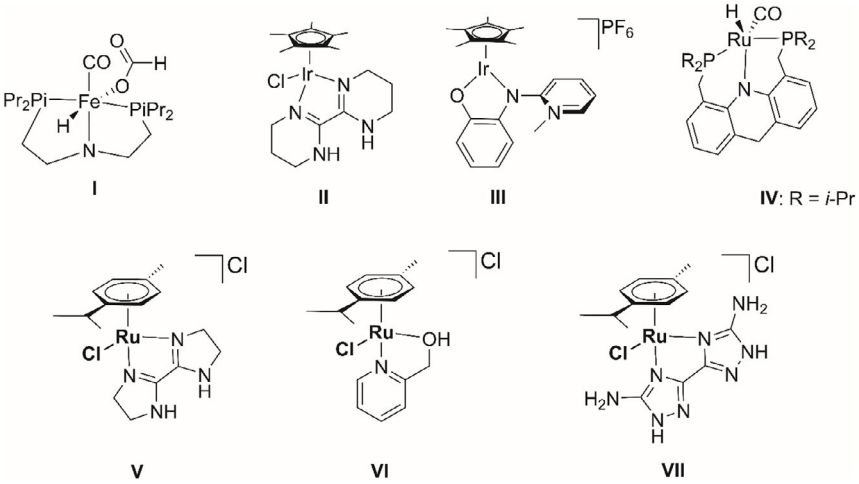

Figure 1. Benchmark metal-based and water-soluble ruthenium-based catalysts for FA dehydrogenation.

ruthenium complex ligated by a diamino-bis(1H-1,2,4-triazole) ligand, **VII**.[19] Using 0.01 mol% of catalyst and 20 mmol of FA at 90 °C, a maximum TOF of 570 hr^{-1} was reached.

Herein, we report a panel of water-soluble cationic half-sandwich ruthenium(II) complexes **C1**–**C11** bearing iminopyridine ligands as active catalyst precursors for H_2 production from FA dehydrogenation in dimethyl sulfoxide (DMSO) and water. Our investigation, utilizing spectroscopic, kinetic, and thermodynamic studies, provides insight into the role the solvent plays in regulating the proton source during hydrogen production. We also demonstrate the reusability and long-term performance of the most active catalyst in our panel.

2. Results and Discussion

2.1. Synthesis and Characterization

As shown in **Scheme 1**, the prepared iminopyridine ligands (**L1**–**L9**) react with the $[Ru(p\text{-cymene})Cl_2]_2$ precursor to afford cationic half-sandwich iminopyridine ruthenium(II) complexes (**C1**–**C11**) in moderate-to-good yields (73%–87%). These complexes, except for **C5**, and **C6**, are air- and moisture-stable yellow solids and display good solubility in polar solvents such as MeOH, H_2O, and DMSO, but poor solubility in hexane and ethers. The ^1H nuclear magnetic resonance (NMR) spectra of the complexes **C1**–**C11** display a singlet for the imine proton in the region $\delta = 8.49$–9.09 ppm, which is considerably downfield compared to the imine proton of the corresponding free ligand, $\delta = 8.31$–8.61 ppm (Section S3, Supporting Information). Additionally, the ^1H NMR resonances corresponding to the coordinated p-cymene ring for **C1**–**C11** appear in the expected region, $\delta = 5.32$–6.31 ppm.[20] In the fourier transform infrared (FT-IR) spectra for complexes **C1**–**C11**, the imine ($\nu_{C=N}$) band appears in the low wavenumber region, 1611–1626 cm^{-1} compared to the free imine ligands, 1627–1649 cm^{-1} (Section S3, Supporting Information). The electrospray ionization mass spectrometry (ESI-MS) spectra of complexes **C1**–**C11** recorded in the positive ion mode showed prominent isotope clusters corresponding to the $[M]^+$ fragment ions (Section S3, Supporting Information). Suitable single crystals of **C1** and **C11** were obtained from the slow

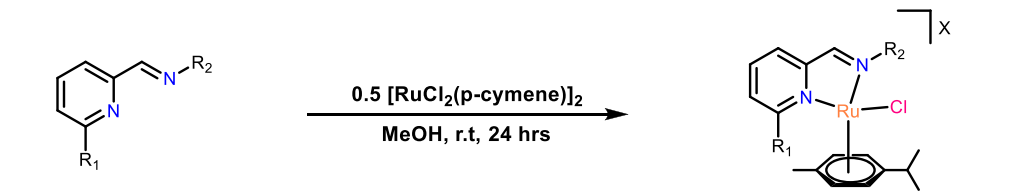

L1 or **C1**: R_1 = H, R_2 = Phenyl, X = Cl
L2 or **C2**: R_1 = H, R_2 = 2,6-dimethylphenyl, X = Cl
L3 or **C3**: R_1 = H, R_2 = 2,6-diisopropylphenyl, X = Cl
L4 or **C4**: R_1 = H, R_2 = Mesityl, X = Cl
L5 or **C5**: R_1 = H, R_2 = Benzyl, X = Cl
L6 or **C6**: R_1 = H, R_2 = Cyclohexyl, X = Cl
L7 or **C7**: R_1 = H, R_2 = Propyl, X = Cl
L8 or **C8**: R_1 = CH_3, R_2 = Phenyl, X = Cl
L9 or **C9**: R_1 = CF_3, R_2 = Phenyl, X = Cl
C10: R_1 = H, R_2 = Phenyl, X= BPh_4
C11: R_1 = H, R_2 = Phenyl, X = PF_6

Scheme 1. Synthesis of cationic half-sandwich iminopyridine Ru(II) complexes **C1**–**C11**.

Research Article
doi.org/10.1002/ejic.202500212

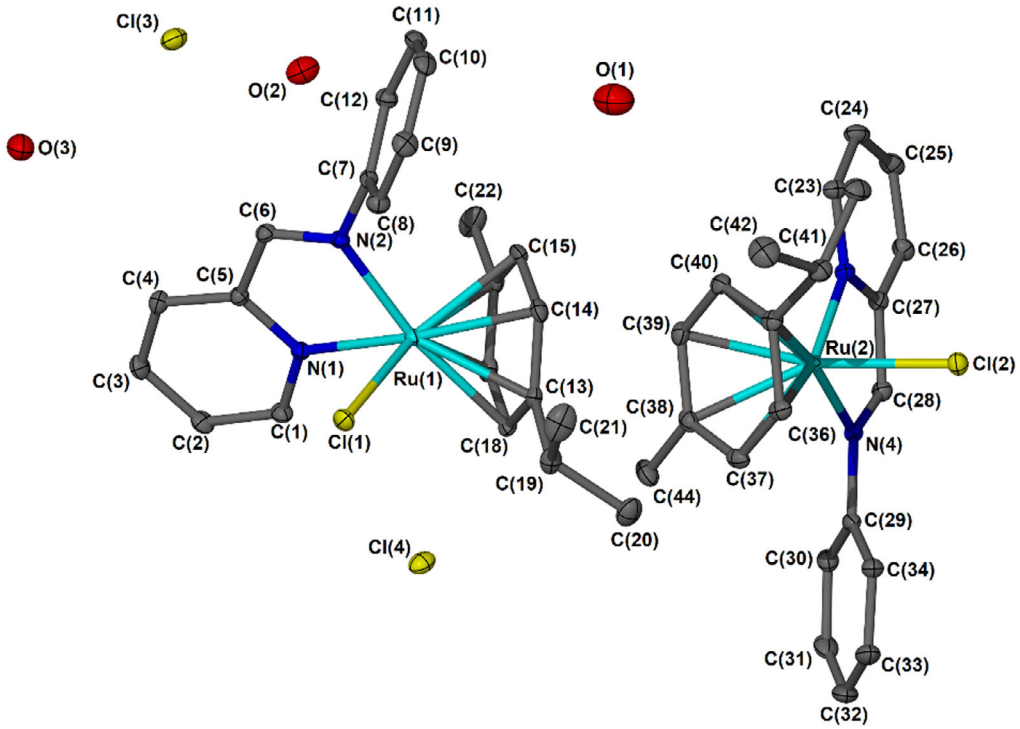

Figure 2. Molecular structure of **C1**, illustrating the two independent molecules in the asymmetric unit cell, with atomic numbering illustrated with 30% probability ellipsoids. All hydrogen atoms are omitted for clarity.

diffusion of diethyl ether in methanolic solutions. The molecular structure of **C1** is illustrated in **Figure 2**, while that of **C11** is provided in Figure S81, Supporting Information. Both complexes crystallized in the triclinic crystal system with the *P-1* space group. The complexes adopt a three-legged piano stool arrangement in which the Ru(II) metal center has a pseudo-octahedral molecular geometry (Figure 2). The coordination sphere around ruthenium is completed by the iminopyridine ligand, which coordinates to the Ru metal center through the N atoms of the imine and the pyridine ring, *p*-cymene ring at the tip of the stool, and a Cl atom at the bottom of the stool. Suitable single crystals of **C1** and **C11** were obtained from the slow diffusion of diethyl ether in methanolic solutions. The molecular structure of **C1** is illustrated in Figure 1, while that of **C11** is provided in Figure S81, Supporting Information. Both complexes crystallized in the triclinic crystal system with the P-1 space group. The complexes adopt a three-legged piano stool arrangement in which the Ru(II) metal center has a pseudo-octahedral molecular geometry (Figure 2). The coordination sphere around ruthenium is completed by the iminopyridine ligand, which coordinates to the Ru metal center through the N atoms of the imine and the pyridine ring, *p*-cymene ring at the tip of the stool, and a Cl atom at the bottom of the stool. The Ru—N_{py} bond lengths, i.e., Ru(1)-N(1), are 2.0961(15) Å and 2.083(2) Å for **C1** and **C11**, respectively. These bond lengths are consistent with the sp^2-hybridized N_{py} and are within the range observed for related ruthenium complexes.[21] The increased rigidity in the complexes is reflected in the N(2)—Ru(1)—N(1) bond angles of 76.43(6)° and 76.75(9)° for **C1** and **C11**, respectively, which deviate from the ideal 90° bond angles for octahedral complexes.

The planar nature, with slight distortion, of the iminopyridine ligands in the complexes is indicated by the Ru(1)—N(1)—C(1)—C(2) torsion angles of 171.98(4)° and 175.1(2)° for **C1** and **C11,** respectively. Key crystallographic details and selected bond parameters are summarized in Table S1, S2, Supporting Information.

2.2. FA Dehydrogenation

No gas evolution was observed when the reaction was conducted without a catalyst or in the presence of the dichloro(*p*-cymene) ruthenium(II) dimer (**Table 1**, entry 1). H_2 gas formation was confirmed by ^{1}H NMR as a singlet at $\delta = 4.61$ ppm in DMSO-d_6 (Figure S82, Supporting Information). The observed chemical shift for H_2 gas is in accordance with the literature precedent.[22] The production of CO_2 with negligible CO formation and the absence of H_2O were confirmed by gas chromatography coupled with thermal conductivity detector analyses, with He as carrier gas (Figure S83, Supporting Information). For complexes **C1**–**C4**, the imine nitrogen is bonded to aromatic substituents bearing different alkyl moieties. The catalysis performed with **C1**, bearing the unsubstituted phenyl ring, yielded the highest amount of $CO_2 + H_2$, i.e., 236 mL, reaching TONs of 483 after 120 minutes (Table 1, entry 2). A drastic decrease in activity was observed when varying the alkyl substitution from **C1** to **C2** (TON = 130) and **C3** (TON = 51) owing to the introduction of successively bulkier methyl and di-isopropyl substituents on the aromatic ring, which hinder FA coordination to the Ru metal center (Table 1, entries 3 and 4). Complex **C4** containing mesityl substituents on the aromatic ring displayed similar catalytic activity as the 2,6-dimethyl-substituted version, **C2** (Table 1, entries 3 and 5).

Research Article
doi.org/10.1002/ejic.202500212

Table 1. Initial screening of iminopyridine Ru(II) complexes C1–**C9**.

Entry[a)]	Catalyst	CO2 + H2 [mL]	TON	TOF [hr^{-1}]	Conversion [%]
1	[Ru(*p*-cymene)Cl_2]$_2$	–	–	–	–
2	C1	236	483	281	91
3	C2	64	130	46	25
4	C3	25	51	21	10
5	C4	72	147	54	28
6	C5	217	444	191	84
7	C6	4	7	5	2
8	C7	36	73	27	14
9	C8	117	238	85	45
10	C9	144	294	123	56

[a)]Conditions: FA (5 mmol, 0.2 mL), **C1**–**C9** (0.2 mol%, 0.01 mmol), HCOONa (1 mmol), DMSO (2 mL), temperature (90 °C), and total reaction volume (2.2 mL). TOF estimated based on gas evolution at 90 mins. TONs and conversion determined at 120 mins. Each reaction was repeated twice with an error of less than 5%. Maximum theoretical volume ($CO_2 + H_2$): 259 mL.

For complexes **C5**–**C7**, the imine nitrogen is bound to a range of aliphatic substituents. Complex **C5** bearing a benzyl substituent exhibited good catalytic activity, i.e., TON = 444 compared to **C6** (TON = 7) and **C7** (TON = 73) bearing cyclohexyl and propyl substituents, respectively (Table 1, entries 6–8). The high activity of **C5** is attributed to the flexibility of the benzyl ring, which enables easy substrate coordination to the metal center. Complexes **C8** and **C9** possess a methyl and a trifluoromethyl substituent on the α carbon of the pyridine ring, respectively. In both cases, introducing these substituents led to decreased catalytic activity, i.e., TON = 238 for **C8** and TON = 294 for **C9**, compared to the analogous unsubstituted complex **C1** with TON of 483 (Table 1, entries 9 and 10). **C9** exhibits slightly higher catalytic performance than **C8** due to the electron-withdrawing trifluoromethyl substituent that increases the electrophilicity of the Ru metal center.

The nature and amount of formate cation exerted a crucial role in facilitating the rate of FA dehydrogenation over **C1**. A reactivity trend K (TON = 499) > Na (TON = 483) > Li (TON = 332) was established when the nature of the alkali formate cation was varied (Figure S84, Supporting Information). This behavior is attributed to the relatively large size of K^+ compared to that of Na^+ and Li^+, which enables easy interaction with the Cl^- ligand of **C1** according to the hard-soft acid-base principle to afford the catalytically active Ru-hydride species. Results indicated that TONs increased with an increase in the amount of potassium ormate (HCOOK) from 0.2 to 1.0 equivalent with respect to FA. Adding excess HCOOK, i.e., 1.4 equivalents, led to the dehydrogenation of formate ($HCOO^-$) upon full consumption of available FA. TONs of 521 are achieved within 50 min for the dehydrogenation of 0.2 mL of FA using 0.6 eq of HCOOK over **C1** under optimized reaction conditions (Figure S85, Supporting Information). Solvent-dependent FA dehydrogenation rates were deduced from performing the reaction in various solvent media. Interestingly, **C1** was soluble and effective in catalyzing FA dehydrogenation in water reaching TONs = 208 after 50 min (Figure S86, Supporting Information). Halving and/or doubling the initial solvent volume (2 mL) led to decreased catalytic activities due to dilution effects associated with high reaction volumes and solubility effects accompanied by low reaction volumes, respectively (Figure S87, Supporting Information). Varying the nature of the ruthenium complex counterion from the less sterically demanding Cl in **C1** to more sterically demanding BPh_4 and PF_6 counterions in **C10** and **C11**, respectively, did not influence either the rate or the amount of FA dehydrogenated (Figure S88, Supporting Information).

2.3. Mechanistic Studies in DMSO

The activation energy (E_A) was obtained by measuring the initial rates of FA consumption from 70 to 100 °C (Figure S89, Supporting Information). The estimated apparent E_A from the Arrhenius plot is 84 kJ/mol (**Figure 3**b), within the range of FA dehydrogenation reactions catalyzed by other noble metals.[23] The activation parameters $\Delta H^{\ddagger} = 81\ kJ\ mol^{-1}$ and $\Delta S^{\ddagger} = -134\ J\ K\ mol^{-1}$ were calculated from the Eyring plot based on the first 60 min of FA consumption (Figure S90, Supporting Information). The highly negative $\Delta S^{\ddagger}$ value points toward an associative rate-determining step, i.e., the interaction of a reaction intermediate with a molecule of FA.[24] The double-logarithmic plots of the initial rates of FA dehydrogenation (2.5 M, 0.2 mL) with the concentration of **C1** (0.025–0.1 mol%) illustrate the first-order dependence between 0.025 and 0.075 mol% (order of 1.30), followed by saturation kinetics at higher concentrations up to 0.2 mol% (Figure S91–S93, Supporting Information).[23] Further, the reaction order of 0.963 for the dehydrogenation of varying concentrations of FA over 0.2 mol% of **C1** at 90 °C evidenced instant coordination of a molecule of FA or formate ions to the Ru metal center to afford [HCOO-Ru] species, i.e., no preequilibrium exists between **C1** and FA (Figure S94–S96, Supporting Information).

The involvement of Ru–hydride species in FA dehydrogenation was evidenced by the presence of multiple ^{1}H NMR signals in the region $\delta = -11$ to -14.5 ppm, indicative of Ru–hydride species from the reaction of **C1** with 1 equivalent of HCOOK in DMSO-d_6 at 90 °C (Figure S97, Supporting Information). The presence of several hydride species is likely due to competing equilibria under these reaction conditions. Next, the catalyst-to-formate ratio was increased to catalytically relevant ratios, i.e., 1:50. Under these reaction conditions, an intense ^{1}H NMR signal was observed at $\delta = -11$ ppm as the major Ru-hydride species during the reaction of **C1** with HCOOK in DMSO-d_6 at 90 °C (Figure S98, Supporting Information). This species was identified as the Ru–monohydride species according to literature precedent.[17,25] Further, kinetic isotope effect (KIE) studies were conducted to gain deeper insight into the catalytic process of FA dehydrogenation over **C1** (**Table 2**). Triethylamine (NEt_3) was employed as the additive to avoid deuterium scrambling. Replacing HCOOH with formic-d acid (DCOOH) had a minimal effect on the reaction rate with KIE = 1.2 (Table 2, entry 2). Employing formic acid-d_2 (DCOOD) as the substrate led to a more pronounced decrease in the reaction rate with KIE = 2.1 (Table 2, entry 3). The KIE effect with formic acid-d (HCOOD) was found to be 1.4, which in comparison to DCOOH suggests a more

Research Article
doi.org/10.1002/ejic.202500212

Chemistry Europe
European Chemical Societies Publishing

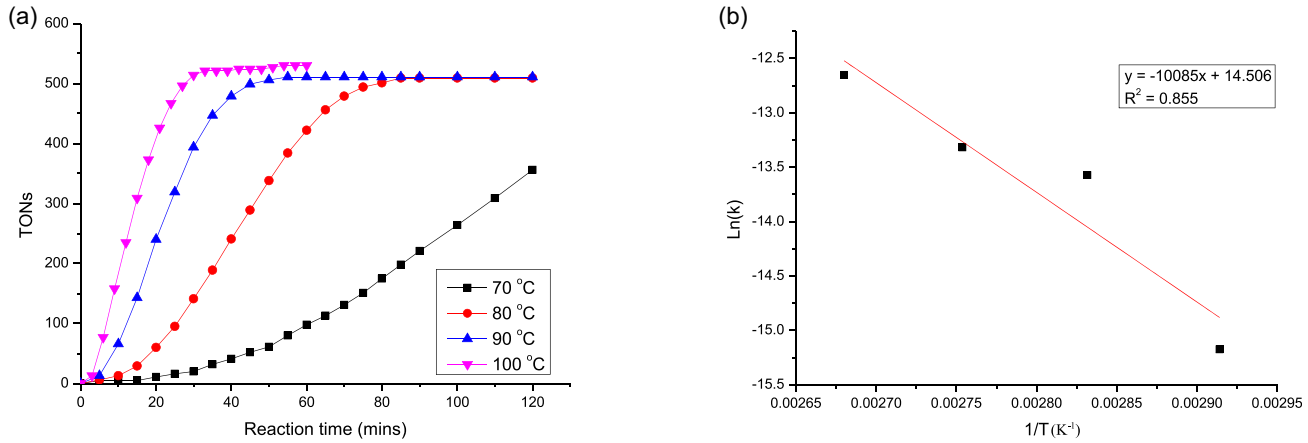

Figure 3. a) Influence of reaction temperature on the activity of **C1** in FA dehydrogenation. Conditions: FA (5 mmol, 0.2 mL), **C1** (0.2 mol%, 0.01 mmol), HCOOK (3 mmol), DMSO (2 mL), temperature (as indicated), and total reaction volume (2.2 mL). b) Arrhenius plot based on FA consumption in the first 60 min of the reaction using **C1**.

Table 2. KIE in the dehydrogenation of FA over catalyst C1 in DMSO.

Entry[a)]	Catalyst	Substrate	Solvent	TOF	KIE
1	C1	HCOOH	DMSO	115	–
2	C1	DCOOH	DMSO	100	1.2
3	C1	DCOOD	DMSO	54	2.1
4	C1	HCOOD	DMSO	85	1.4

[a)]Conditions: FA (1.33 mmol, 0.05 mL), **C10** (0.2 mol%, 0.00266 mmol), NEt_3 (1 mmol), DMSO (1 mL), and temperature (80 °C). TOF measured at 30 mins. KIE = $TOF_{HCOOH}/TOF_{isotopologue}$).

pronounced effect of protonation and/or O—H bond cleavage. The KIE data, in combination with the highly negative entropy of activation and first-order dependence in [FA], suggests that the rate-determining step likely involves the cleavage of the O—H bond and/or the protonation of the Ru—hydride intermediate. The observed trend corroborates well with the literature precedent for reactions catalyzed in DMSO.[13]

2.4. Mechanistic Studies in Water

The activation energy (E_A) was obtained by measuring the initial rates of FA consumption from 70 to 100 °C (Figure S99, Supporting Information). The estimated apparent E_A from the Arrhenius plot is 108 kJ mol^{-1} (**Figure 4**b), within the range of FA dehydrogenation reactions catalyzed by noble metals.[23] The obtained E_A is ≈24 kJ mol^{-1} higher than the E_A determined from the reactions performed in DMSO. From the Eyring analyses (Figure S100, Supporting Information), the activation parameters $\Delta H^{\ddagger} = 105$ kJ mol^{-1} and $\Delta S^{\ddagger} = -75$ J K mol^{-1} were calculated. As in DMSO, the rate-determining step for the reaction performed in H_2O is associative as indicated by the negative $\Delta S^{\ddagger}$ value. A linear dependence (reaction order = 0.924) was deduced from the double-logarithmic plot of the initial rates of FA consumption with **C1** concentration (0.025–0.1 mol%) and points toward the generation of the monomeric species of **C1** as the most active catalytic species and the absence of dimeric species during the catalytic dehydrogenation of FA (Figure S101–S103, Supporting Information). From the double-logarithmic plot of the initial rates of FA consumption with the concentration of FA (0.05–0.2 mL), a positive reaction order of 0.306 was obtained (Figure S104–S106, Supporting Information). Interestingly and in contrast to observations in DMSO, performing the catalytic reaction in water leads to the existence of a pre-equilibrium between the **C1** and FA as well as the interaction of FA or formate ions with the Ru metal center. Usually, half-order reaction kinetics with respect to FA concentration indicate equimolar interaction of the FA substrate with the Ru complex.[18,23] This difference in Ru–FA interactions is also reflected in the more positive $\Delta S^{\ddagger}$ value in water ($\Delta S^{\ddagger} = -134$ J K mol^{-1} in DMSO) and implies divergent species participating in the hydrogen-formation step. Our kinetic and thermodynamic data suggest that FA is involved in the hydrogen formation step in DMSO,[13] whereas hydronium (H_3O^+) ions are involved when generating H_2 in water.[17]

KIE studies were conducted to better understand the role of formate activation versus hydrogen evolution on the rate of FA dehydrogenation (**Table 3**). The observed trend in KIE measurements indicated that both d_2-FA (DCOOD, KIE 1.9) and HCOOD (KIE 1.9) were more influential than D_2O (KIE 1.1) on the reaction rate for FA dehydrogenation over **C1** under the reaction conditions in Table 3. Crucially, replacing HCOOH with DCOOH led to a more pronounced KIE of 6.0 in H_2O. These results, in combination with kinetic and thermodynamic data, infer that the rate-determining step involves C–H bond cleavage during decarboxylation of the Ru-formato species to yield the Ru–hydride species, rather than the proton (H^+)-assisted hydrogen gas evolution.[26,27] The dehydrogenation of FA in the presence of DCOOD and/or D_2O may involve a complex combination of reaction kinetics, equilibria, and isotope exchange processes, leading to the slightly low KIE values shown in Table 3. Nonetheless, the obtained data follows literature precedent. For instance, Himeda and coworkers reported a KIE of 1.6 when D_2O replaced H_2O and a KIE of 2.3 when DCOOD replaced HCOOH.[28] Our analysis of the mechanistic features in DMSO and water allows us to propose

Research Article
doi.org/10.1002/ejic.202500212

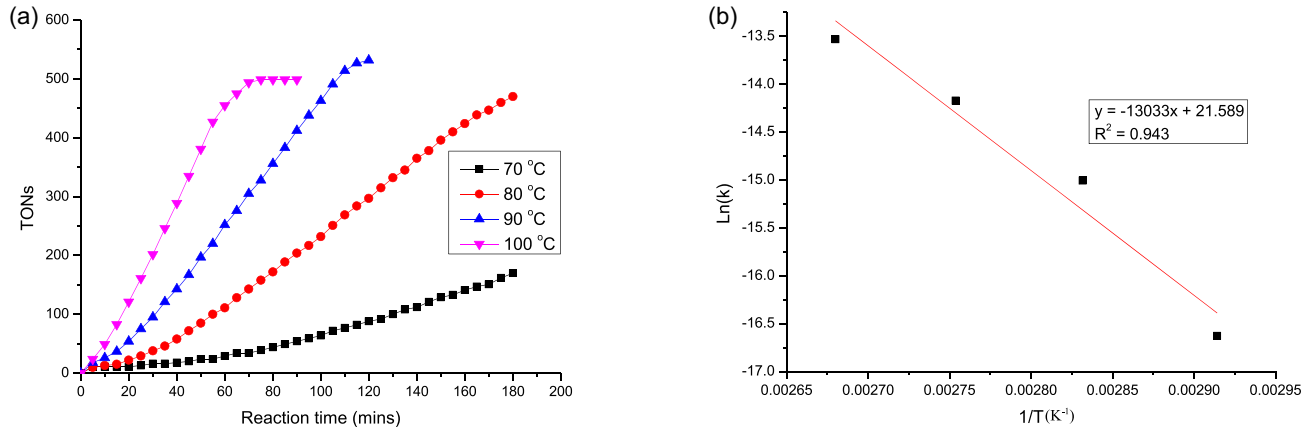

Figure 4. a) Influence of reaction temperature on the activity of **C1** in FA dehydrogenation. Conditions: FA (5 mmol, 0.2 mL), **C1** (0.2 mol%, 0.01 mmol), HCOOK (3 mmol), H_2O (2 mL), temperature (as indicated), and total reaction volume (2.2 mL). b) Arrhenius plot based on FA consumption in the first 60 min of the reaction using **C1**.

Table 3. KIE in the dehydrogenation of FA over catalyst C1 in water.

Entry[a)]	Catalyst	Substrate	Solvent	TOF	KIE
1	C1	HCOOH	H_2O	375	–
2	C1	HCOOH	D_2O	329	1.1
3	C1	DCOOD	H_2O	231	1.6
4	C1	DCOOD	D_2O	202	1.9
5	C1	HCOOD	H_2O	196	1.9
6	C1	HCOOD	D_2O	110	3.4
7	C1	DCOOH	H_2O	63	6.0
8	C1	DCOOH	D_2O	98	3.8

[a)]Conditions: substrate (1.33 mmol, 0.05 mL), **C10** (0.2 mol%, 0.00266 mmol), NEt_3 (1 mmol), solvent (1 mL), and temperature (80 °C). TOF measured at 40 min. KIE = $TOF_{HCOOH}/TOF_{isotopologue}$).

divergent hydrogen production pathways. In DMSO, hydrogen production proceeds with FA as the hydrogen source, which is preceded by Ru-hydride formation from the Ru-formato, with the rate-determining step likely being O—H bond cleavage during the protonation step [**Scheme 2**, pathway a)]. In contrast, in water, hydrogen production proceeds with hydronium ions as the hydrogen source, with decarboxylation to generate Ru-hydride as the rate-determining step [Scheme 2, pathway b)]. Both pathways share Ru-hydride as the resting state.

2.5. Optimized Catalytic Performance

To determine the reusability and long-term stability of **C1** in DMSO, fresh batches of 0.1 mL FA were added to the reaction solution in 30-minute intervals, i.e., time taken to consume the initial amount of FA added into the system. Under the optimized reaction conditions shown in **Figure 5**, the total volume of gas generated decreased with each FA refill (Figure 5a). During the reaction, TOFs of about 1636 hr^{-1} were attained at the end of the initial addition and halved to 837 hr^{-1} at the end of the sixth refill, with estimated TONs of 3000 (Figure S107, Supporting Information). This drastic reduction in activity can be attributed to possible catalyst deactivation due to pH changes associated with the consumption of the substrate and further drastic pH changes during FA refills. To further explore the robustness of catalyst **C1**, FA was continually introduced using an automatic syringe pump at the rate of its consumption, i.e., 0.003 mL min^{-1}. The catalytic rate decreased with time, with TOFs of 540 hr^{-1} reached in the first hour of the reaction decreasing to 199 hr^{-1} after 5 h. Figure 5b indicates the plateau in the generated TONs as a function of time with maximum TONs of 1009 after 5 h under the optimized reaction conditions. These results further reinforce the pH sensitivity of **C1** when DMSO is employed as a solvent medium.

Similarly, the reusability and long-term stability of **C1** for FA dehydrogenation in water were evaluated. **C1** was subjected to repeated 0.1 mL FA injections every 80 min under the reaction conditions shown in **Figure 6**. To our delight, **C1** could dehydrogenate 0.1 mL batches of FA for seven cycles without losing activity, achieving TONs = 7872 at the end of the seventh cycle. TOFs of 682 hr^{-1} were obtained after complete dehydrogenation of the initial FA addition and amounted to 844 hr^{-1} at the end of the seventh refill of FA, illustrating the retained activity of **C1** with each FA injection. This sustained catalytic activity can be attributed to the ability of **C1** to withstand rigorous pH changes associated with the addition and/or consumption of the FA substrate in a water solvent medium. Under these reaction conditions, sustained activity with TONs 13 791 could be obtained within 21 h, before deactivation was observed. Further, the suitability of **C1** for long-term applications was evaluated by injecting FA at a constant rate (0.00125 mL min^{-1}) equal to its consumption in the reaction. Under the optimized reaction conditions shown in Figure S108, Supporting Information, catalyst **C1** was able, although with diminished catalytic activity (TOF = 43 hr^{-1}), to catalyze the dehydrogenation of FA for over 34 h. These results further reinforce the increased stability of the catalytic species of **C1** in water. The decreased catalytic activity under these conditions is likely due to the reaction not proceeding at the desired pH range, i.e., highly basic conditions due to the excess HCOOK in the reaction solution.

Research Article
doi.org/10.1002/ejic.202500212

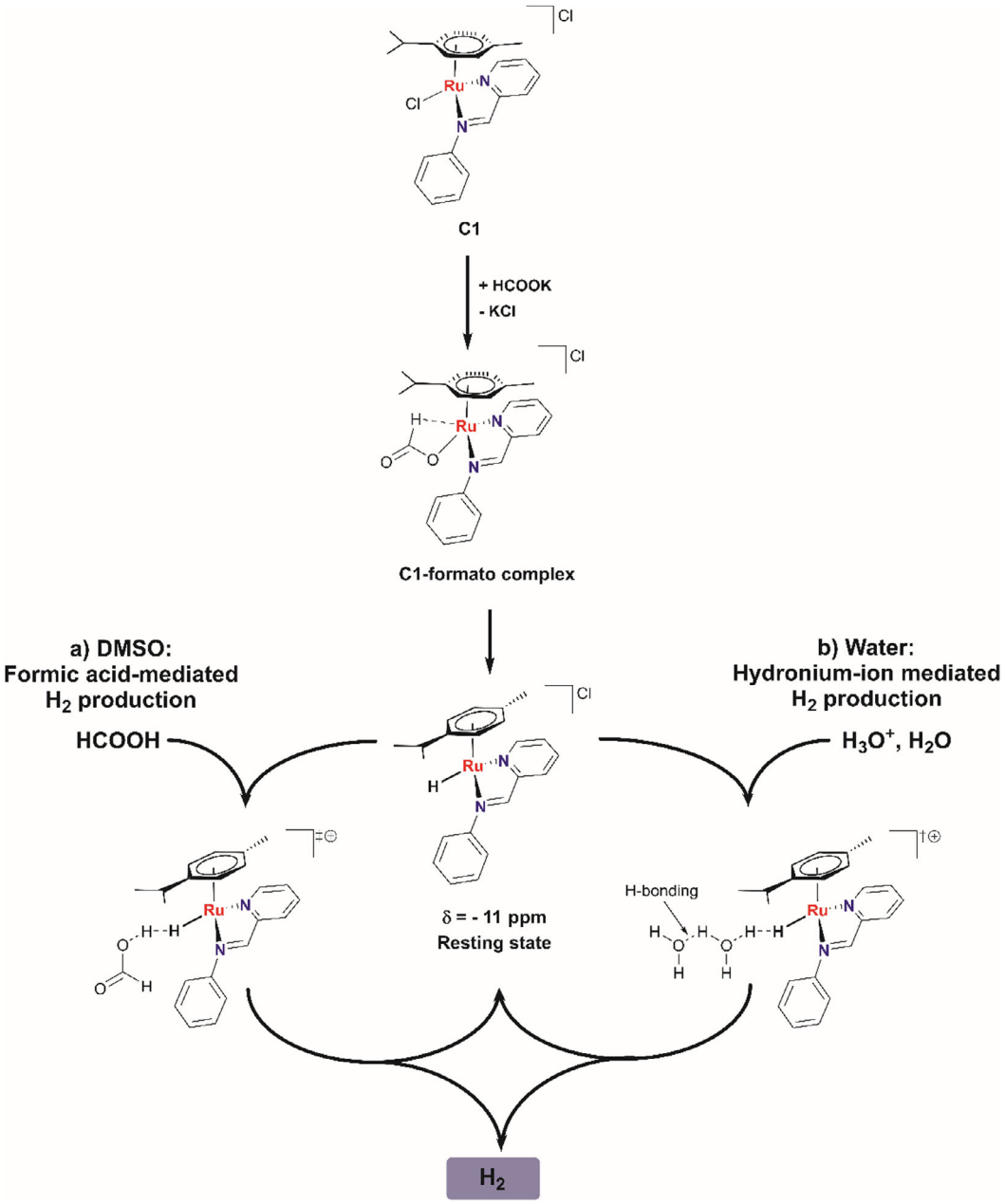

Scheme 2. Divergent hydrogen production pathways, for the dehydrogenation of FA using **C1** in a) DMSO and b) water.

2.6. Comparative Analysis with Reported Catalytic Systems

In this section, the performance of Ru catalyst **C1** toward FA dehydrogenation is compared with reported ruthenium complexes operated under similar reaction conditions. Table S3 and Figure S109, Supporting Information, summarize the catalytic performance of the existing literature work and compare it to the work presented in this study. As described previously, compounds **I–IV** (Figure 1) represent benchmark catalysts, which outperform most catalysts, based on both earth-abundant and platinum group metals (PGMs). In addition, Huang and coworkers reported a highly efficient Ru complex **VIII** that achieved maximum TONs of 1 100 000 in DMSO after 150 h, attributable to enhanced stabilization by the tridentate noninnocent PNP ligand framework (Table S3, Supporting Information, entry 1).[29] The best-performing Ru-catalyst in water was reported by Huang and co-workers, **V**, reaching TONs of 350 000 and TOFs of 12 000 hr^{-1} (Figure 1,V).[17] Catalyst **C1** was found to outperform several reported Ru- and other metal-containing systems. For instance, Singh and coworkers reported a Ru complex, **VI**, which attained TONs of 6050 and TOFs of 1548 in water (Figure 1, **VI**).[18] In another report, Singh and coworkers illustrated a Ru catalyst system, **IX**, that reached TONs of 2248 in 15 min with reasonably high TOFs of 940 hr^{-1} (Table S3, Supporting Information, entry 2).[30] **C1** outperformed our recently reported Ru-catalysts bearing 1) pyridyl-formamidine ligands, **X**, and 2) pyridyl-pyrazolyl ligands, **XI**, which in the presence of formate could dehydrogenate FA with TONs and TOFs of 7892 and 225 hr^{-1}

Research Article
doi.org/10.1002/ejic.202500212

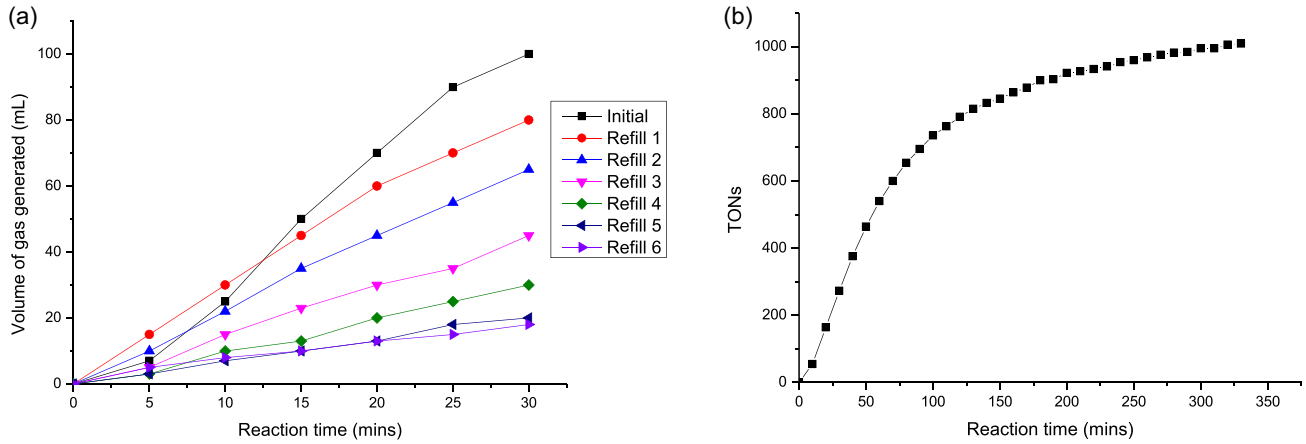

Figure 5. a) Stacked plots of the gas evolution upon repetitive FA addition with $t = 0$ mins for each addition. b) Influence of continuous FA injections on the rate of FA dehydrogenation. Conditions: FA (2.5 mmol, 0.1 mL), **C1** (0.1 mol%, 0.0025 mmol), HCOOK (3 mmol), DMSO (2 mL), temperature (90 °C), and total reaction volume (2.1 mL).

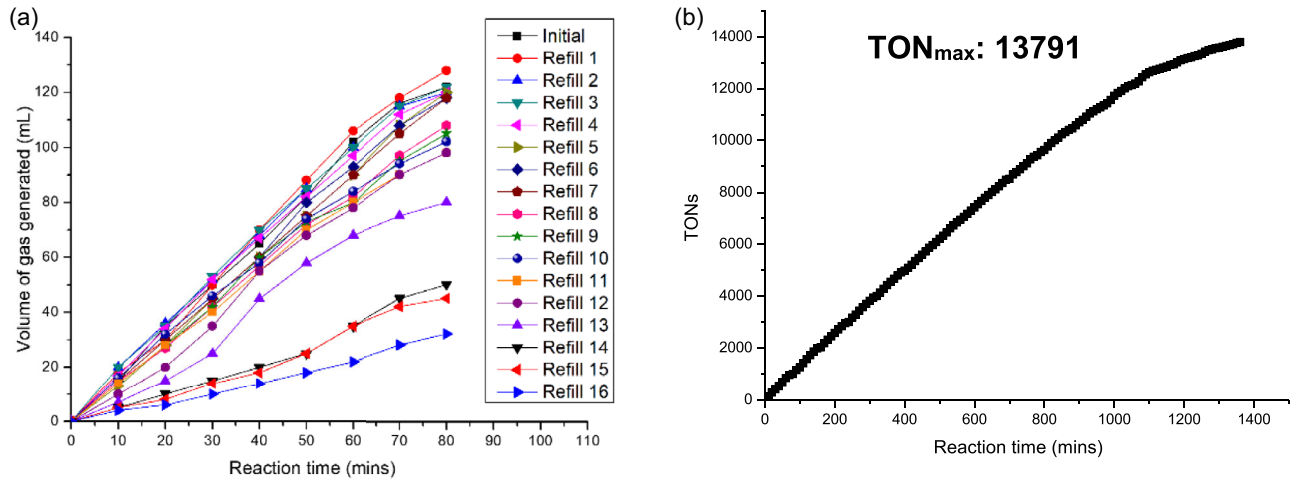

Figure 6. a) Stacked plots of the gas evolution upon repetitive FA addition with $t = 0$ mins for each addition. b) Influence of repetitive FA injections on the rate of FA dehydrogenation. Conditions: FA (2.5 mmol, 0.1 mL), **C1** (0.1 mol%, 0.0025 mmol), HCOOK (3 mmol), H_2O (2 mL), temperature (90 °C), and total reaction volume (2.1 mL).

and 3169 and 336 hr^{-1}, respectively (Table S3, Supporting Information, entries 3 and 4).[31,32] The better performance of **C1** may be attributable to both its faster activation and enhanced stability under operating conditions. A π-coordinated phenoxy-ligated Ru-dimer, **XII**, was active for FA dehydrogenation at 90 °C, generating TONs of 173 and $TOF_{initial}$ of 202 h^{-1} in DMSO (Table S3, Supporting Information, entry 5).[33] The lower performance of **XII** may be ascribed to its sensitivity to water, leading to catalyst inhibition. The $[Ru(triphos)(MeCN)_3](OTf)_2$ system, **XIII**, was reported to achieve full conversion in an hour, at low catalyst loadings with N,N-dimethyloctanamine as additive, achieving TONs and TOFs of 10 000 and 1000 h^{-1}, respectively (Table S3, Supporting Information, entry 6), with slower activation kinetics translating into TONs and TOFs of 1000 and 100 h^{-1} after 180 min.[34] The PCP-Ni(II)-hydride, **XIV**, dehydrogenated FA in the presence of triethylamine at 80 °C, with TONs of 626 (Table S3, Supporting Information, entry 7) and was found to generate product gas with higher CO_2 content than expected, attributed to propylene carbonate cleavage as a side reaction.[35] A related (PNP)Ir(III)-trihydride complex, **XV**, catalyzed the dehydrogenation of FA in acidic water, with pH-dependent activity. The best activity displayed a TOF_{max} of 1880 h^{-1} at pH 2.8, with catalyst deactivation observed at lower pH (Table S3, Supporting Information, entry 8).[36] Compound **XVI**, a P_4-tetradentate tetraphos-ligated Fe(II) tetrafluoroborate complex, dehydrogenated FA under base-free conditions in propylene carbonate at 60 °C (Table S3, Supporting Information, entry 9).[37] TONs of 6061 were obtained after 6 h of reaction, with $TOF_{initial}$ of 1737 h^{-1}. Finally, the $[BrMn(L)(CO)_3]$ complex, (L = 2-(4,5-dihydro-1H-imidazol-2-yl)pyridine), **XVII**, reported by Beller dehydrogenated FA under continuous-flow conditions, with TON of 5476 after 45 h and TOF up to 192 h^{-1} after 3 h.[38] Our catalyst system provides efficient dehydrogenation activity, combined with ease-of-synthesis, modularity in terms of electronic and steric properties, as well as sustained activity in water. These are distinguishing features which can be exploited in future catalyst design strategies.

Research Article
doi.org/10.1002/ejic.202500212

3. Conclusion

A series of iminopyridine ruthenium complexes, **C1–C11,** were evaluated for FA dehydrogenation, where the catalytic activity was closely linked to the nature of the substituent on the imine nitrogen of the ligands. Catalyst **C1** was found to be most effective, reaching TONs of 483 after 2 h. The activity of **C1** toward FA dehydrogenation was solvent-dependent with $E_A = 81$ kJ mol^{-1} in DMSO and $E_A = 108$ kJ mol^{-1} in water. The main Ru-hydride species responsible for FA dehydrogenation was observed at $\delta = -11$ ppm using ^{1}H NMR experiments. KIE experiments identified the protonation of Ru-hydride species and the decarboxylation of Ru-formato species as the turnover-limiting steps in DMSO and water, respectively. The hydrogen source was found to be solvent dependent, with FA involved in the hydrogen formation step in DMSO, whereas hydronium (H_3O^+) ions are involved when generating H_2 in water. Complex **C1** was observed to be more stable in water than DMSO, achieving TONs of 13 791 with loss of activity commencing after 16 cycles. Under continuous FA addition, **C1** was active, although with reduced performance (TOF = 43 hr^{-1}), for over 34 h in water.

4. Experimental Section

General Considerations

All reactions involving air- and/or moisture-sensitive compounds were performed under purified dry nitrogen using normal Schlenk techniques. All reagents were obtained from Sigma-Aldrich and used as received. Solvents were purchased from Promark Chemicals and freshly dried before use. IR spectra were recorded as neat oils or solids on a Bruker Tensor 27 FT-IR spectrometer fitted with an attenuated total reflection (ATR) accessory. NMR spectra were recorded on a Bruker Avance NMR spectrometer (^{1}H at 400 MHz,^{13}C at 101 MHz). ESI-MS analyses were recorded on a Thermo Scientific Dionex Ultimate 3000 UHPLC coupled to a Bruker Compact QqTOF HRMS. Elemental analysis was recorded using a Thermo Scientific Flash 2000 Series CHNS-O Analyzer, at the University of Johannesburg, as a service.

All the ligands, except for **L9**, have previously been reported and were prepared according to the reported literature methods, as described in the Supplementary Information. Representative synthesis of **C1** is provided below. The remainder is described in the Supplementary Information.

General Considerations: [(L1)RuCl(p-Cymene)]Cl, C1

Ligand **L1** (47.8 mg, 0.26 mmol) was added to a stirred solution of $[RuCl_2(p\text{-cymene})]_2$ (80.4 mg, 0.13 mmol) in MeOH (10 mL), and the resulting solution was reacted for 24 h at room temperature under a N_2 atmosphere. After the reaction, the solution was concentrated to 1 mL, redissolved in DCM (10 mL), and layered with excess diethyl ether to afford the product as a yellow crystalline solid (145.1 mg, 87%). **^{1}H NMR** (400 MHz, DMSO-d$_6$): δ (in ppm) = 9.69 (d, J = 5.7 Hz, 1H), 9.08 (s, 1H), 8.37–8.32 (m, 2H), 7.88–7.81 (m, 3H), 7.63 (m, 3H), 6.12 (d, J = 6.2 Hz, 1H), 5.82 (d, J = 6.2 Hz, 1H), 5.64 (m, 2H), 2.15 (s, 3H), 0.98 (d, J = 7.1 Hz, 6H).**^{13}C NMR** (101 MHz, DMSO-d$_6$): δ (in ppm) = 167.99, 156.19, 154.58, 151.71, 139.88, 130.19, 129.72, 129.50, 128.91, 122.53, 105.05, 103.31, 86.59, 86.10, 85.11, 84.99, 30.45, 21.69, 21.60, 18.27. **FT-IR** (ATR, neat): 1612.64 cm^{-1} ($\nu_{C=N}$), 1587.62 cm^{-1} ($\nu_{pyr\text{-}C=N}$). **HRMS (ESI)** *m/z* calcd for $C_{22}H_{24}ClN_2Ru^+$: 453.00 [M]$^+$; found: 453.0669. Anal. calcd. for $C_{22}H_{24}Cl_2N_2Ru$: C 54.10; H 4.95; N 5.74. Found: C 54.03; H 5.16; N 5.63.

General Considerations: Procedure for Catalytic FA Dehydrogenation

A stock solution of the complex in DMSO or H_2O was prepared. From the stock solution, the desired quantity of complex was added to a Schlenk flask followed by the addition of HCOOM (where M = Li, Na, K). The flask was sealed with a rubber septum, and the atmosphere was exchanged for N_2. The reaction solution was stirred at 800 rpm for 5 min at room temperature. Then, FA was added, and the mixture was stirred for an additional minute. Lastly, the reaction mixture was heated at the desired temperature using a preheated oil bath and the gas evolution was monitored using an inverted graduated measuring cylinder. For the continuous FA addition experiment, a similar approach was used, and an NE-300 Just Infusion syringe pump was used to inject FA from a Hamilton syringe fitted with a long metallic needle directly after the immersion of the reaction flask in the oil bath.

X-Ray Crystal Structure Determination

Single-crystal X-ray diffraction data were collected on a Bruker APEX-II CCD diffractometer. The crystal was kept at 173.00 K during data collection. Using Olex2,[39] the structure was solved with the SHELXT[40] structure solution program using intrinsic phasing and refined with the SHELXL[41] refinement package using least-squares minimization. All nonhydrogen atoms were refined anisotropically, while hydrogen atoms were placed in calculated positions using riding models. High-resolution molecular diagrams were generated with POV-ray.[42] Deposition Numbers 2 423 518 (for **C1**) and 2 423 519 (for **C2**), contain the supplementary crystallographic data for this paper. These data are provided free of charge by the joint Cambridge Crystallographic Data Centre and Fachinformationszentrum Karlsruhe Access Structures service.

Acknowledgements

The authors gratefully thank the School of Chemistry, University of the Witwatersrand, for infrastructure and equipment support, Prof. Manuel Fernandes (Wits University) for his assistance with SCXRD analyses, and Sasol South Africa for its financial support to TIM and RM. A.J.S acknowledges funding support of the National Research Foundation (ZA), with grant numbers 137758, 127291, and CPRR240312208672.

Conflict of Interest

The authors declare no conflict of interest.

Author Contributions

Thabiso Mphuti: investigation (lead); methodology (lead); writing—original draft (lead). **Rotondwa Mphephu**: investigation (supporting); methodology (supporting); writing—original draft (supporting). **Moegamat Joseph**: formal analysis (supporting); writing—review and editing (supporting). **Andrew J. Swarts**: funding acquisition (lead); project administration (lead); resources (lead); supervision (lead); writing—review and editing (lead).

Data Availability Statement

The data that support the findings of this study are available in the supplementary material of this article.

Keywords: dehydrogenation · hydrogen · iminopyridines · ruthenium

[1] M. R. Usman, *Renew. Sustain. Energy Rev.* **2022**, *167*, 112743.
[2] P. M. Modisha, C. N. M. Ouma, R. Garidzirai, P. Wasserscheid, D. Bessarabov, *Energy Fuels.* **2019**, *33*, 2778.
[3] D. Mellmann, P. Sponholz, H. Junge, M. Beller, *Chem. Soc. Rev.* **2016**, *45*, 3954.
[4] R. S. Coffey, *Chem. Commun. London* **1967**, 923.
[5] H. Jeon, Y.-H. Chung, *Appl. Catal. B* **2017**, *210*, 212.
[6] J. L. Santos, C. Megías-Sayago, S. Ivanova, M. A. Centew, J. A. Odriozola, *Chem. Eng. J.* **2021**, *420*, 127641.
[7] S. Kar, M. Rauch, G. Leitus, Y. Ben-David, D. Milstein, *Nat. Catal.* **2021**, *4*, 193.
[8] N. H. Anderson, J. Boncella, A. M. Tondreau, *Chem. Eur. J.* **2019**, *25*, 10557.
[9] B. Loges, A. Boddien, H. Junge, M. Beller, *Angew. Chem., Int. Ed.* **2008**, *47*, 3962.
[10] C. Fellay, J. Dyson, G. Laurenczy, *Angew. Chem. Int. Ed.* **2008**, *47*, 3966.
[11] E. A. Bielinski, P. O. Lagaditis, Y. Zhang, B. Q. Mercado, C. Würtele, W. H. Bernskoetter, N. Hazari, S. Schneider, *J. Am. Chem. Soc.* **2014**, *136*, 10234.
[12] Z. Wang, S.-M. Lu, J. Li, J. Wang, C. Li, *Chem. - Eur. J.* **2015**, *21*, 12592.
[13] N. Lentz, M. Albrecht, *ACS Catal.* **2022**, *12*, 12627.
[14] K. Sordakis, C. Tang, L. K. Vogt, H. Junge, P. J. Dyson, M. Beller, G. Laurenczy, *Chem. Rev.* **2018**, *118*, 372.
[15] A. Wang, P. He, J. Wu, N. Chen, C. Pan, E. Shi, H. Jia, T. Hu, K. He, Q. Cai, R. Shen, *Energy Fuels* **2023**, *37*, 17075.
[16] I. Dutta, S. Chatterjee, H. Cheng, R. K. Parsapur, Z. Liu, Z. Li, E. Ye, H. Kawanami, J. S. E. Low, Z. Lai, X. J. Loh, K.-W. Huang, *Adv. Energy Mat.* **2022**, *12*, 2103799.
[17] C. Guan, D.-D. Zhang, Y. Pan, M. Iguchi, M. J. Ajitha, J. Hu, H. Li, C. Yao, M.-H. Huang, S. Min, J. Zheng, Y. Himeda, H. Kawanami, K.-W. Huang, *Inorg. Chem.* **2017**, *56*, 438.
[18] S. Patra, S. K. Singh, *Inorg. Chem.* **2020**, *59*, 4234.
[19] S. Ge, J.-H. Liu, L. Gong, X.-F. Mo, C. Liu, X.-Y. Yi, P. He, *Eur. J. Inorg. Chem.* **2024**, *27*, e202300509.
[20] C. Binnani, R. K. Rai, D. Tyagi, S. M. Mobin, S. K. Singh, *Eur. J. Inorg. Chem.* **2018**, *2018*, 1435.
[21] P. A. Scattergood, U. Khushnood, A. Tarig, D. J. Cooke, C. R. Rice, P. I. P. Elliott, *Inorg. Chem.* **2016**, *55*, 7787.
[22] G. R. Fulmer, A. J. M. Miller, N. H. Sherden, H. E. Gottlieb, A. Nudelman, B. M. Stoltz, J. E. Bercaw, K. I. Goldberg, *Organometallics* **2010**, *29*, 2176.
[23] A. Boddien, D. Mellmann, F. Gärtner, R. Jackstell, H. Junge, P. J. Dyson, G. Laurenczy, R. Ludwig, M. Beller, *Science* **2011**, *333*, 1733.
[24] S. Upadhyay, *Chemical Kinetics and Reaction Dynamics*, Springer, Netherlands **2006**, pp. 46–54.
[25] C. Fellay, N. Yan, P. J. Dyson, G. Laurenczy, *Chem. Eur. J.* **2009**, *15*, 3752.
[26] Z. J. Wang, S. M. Lu, J. Li, J. J. Wang, C. Li, *Chem. Eur. J.* **2015**, *21*, 12592.
[27] W. H. Wang, J. F. Hull, J. T. Muckerman, E. Fujita, T. Hirose, Y. Himeda, *Chem. Eur. J.* **2012**, *18*, 9397.
[28] W. H. Wang, S. Xu, Y. Manaka, Y. Suna, H. Kambayashi, J. T. Muckerman, E. Fujita, Y. Himeda, *ChemSusChem* **2014**, *7*, 1976.
[29] Y. Pan, C. L. Pan, Y. Zhang, H. Li, S. Min, X. Guo, B. Zheng, H. Chen, A. Anders, Z. Lai, J. Zheng, K.-W. Huang, *Chem. Asian J.* **2016**, *11*, 1357.
[30] S. Patra, M. K. Awasthi, R. K. Rai, H. Deka, S. M. Mobin, S. K. Singh, *Eur. J. Inorg. Chem.* **2019**, *2019*, 1046.
[31] J. M. Edor, M. C. Joseph, J. H. L. Jordaan, H. C. M. Vosloo, A. J. Swarts, *Appl. Organomet. Chem.* **2025**, *39*, e70016.
[32] R. Mphephu, M. C. Joseph, A. J. Swarts, *Eur. J. Inorg. Chem.* **2025**, *28*, e202500063.
[33] R. Verron, E. Puig, P. Sutra, A. Igau, C. Fischmeister, *ACS Catal.* **2023**, *13*, 5787.
[34] I. Mellone, M. Peruzzini, L. Rossi, D. Mellmann, H. Junge, M. Beller, L. Gonsalvi, *Dalton Trans.* **2013**, *42*, 2495.
[35] S. Enthaler, A. Brück, A. Kammer, H. Junge, E. Irran, S. Gülak, *ChemCatChem* **2015**, *7*, 65.
[36] R. Tanaka, M. Yamashita, K. Nozaki, *J. Am. Chem. Soc.* **2009**, *131*, 14168.
[37] F. Bertini, I. Mellone, A. Ienco, M. Peruzzini, L. Gonsalvi, *ACS Catal.* **2015**, *5*, 1254.
[38] A. Léval, A. Agapova, C. Steinlechner, E. Alberico, H. Junge, M. Beller, *Green Chem.* **2020**, *22*, 913.
[39] O. V. Dolomanov, L. J. Bourhis, R. J. Gildea, J. A. K. Howard, H. Puschmann, *J. Appl. Cryst.* **2009**, *42*, 339.
[40] G. M. Sheldrick, *Acta Cryst.* **2015**, *A71*, 3.
[41] G. M. Sheldrick, *Acta Cryst.* **2015**, *C71*, 3.
[42] POV-Ray, Version 3.7, Williamstown, Australia, Persistence of vision ray.

Manuscript received: April 21, 2025
Revised manuscript received: June 12, 2025
Version of record online: June 18, 2025